Slow-light soliton beam splitters

Chong Shou[1] and Guoxiang Huang[1,2,3]
[1]*State Key Laboratory of Precision Spectroscopy, East China Normal University, Shanghai 200062, China*
[2]*NYU-ECNU Joint Institute of Physics at NYU-Shanghai, Shanghai 200062, China*
[3]*Collaborative Innovation Center of Extreme Optics, Shanxi University, Taiyuan 030006, China*

(Received 5 November 2018; published 16 April 2019)

We propose a scheme to realize slow-light soliton beam splitters by using a tripod-type four-level atomic system. We show that optical solitons, which have ultraslow propagation velocity and ultralow generation power, can be generated in the system via electromagnetically induced transparency and can be stored and retrieved with high efficiency and fidelity. In particular, a nonlinear beam splitter that splits one optical soliton into two or more ones can be obtained by switching on and off of two or more control laser fields subsequently. The results reported here open a route not only for active manipulation of nonlinear optical pulses in multistate quantum systems but also for promising applications in optical information processing and transmission.

DOI: 10.1103/PhysRevA.99.043821

I. INTRODUCTION

Optical beam splitters are basic devices that can split an incident optical beam or pulse into two or more beams or pulses in space and/or time domains, which may or may not have the same light power. Optical beam splitters play significant roles in modern physics; especially, they are crucial parts of most interferometers, widely exploited in both thought and real-world physical experiments in the areas of quantum theory, relativity theory, and many other fields of physics and engineering [1,2].

In recent years, much attention has been paid to slow-light beam splitters and their extension [3–24] via electromagnetically induced transparency (EIT) [25] in various multilevel atomic systems that resonantly interact with three or more laser fields. In addition to the interest for fundamental research, the study of slow-light beam splitters has potential applications in both classical and quantum information processing and communication networks. For instance, they can be used to design dynamically reconfigurable all-optical routers and to produce highly efficient entanglement for quantum repeaters [3–27]. However, all works on EIT-based slow-light beam splitters reported up to now are only for linear optical pulses, which may generally experience serious deformation since these optical pulses interact with atoms in a resonant way and hence significant dispersion is generally unavoidable. Thus it is desirable to seek techniques to balance the dispersion and hence to obtain optical pulses that have better performance for the design of slow-light beam splitters. One method of such techniques is to make the system work in weak nonlinear optics regimes.

In this paper, we present a proposal for realizing slow-light soliton beam splitters by exploiting a tripod-type four-level atomic system coupled with two control laser fields and a weak nonlinear probe laser field. We show that optical solitons with ultraslow propagating velocity and ultraslow light power can be created via EIT and they can be stored and retrieved with high efficiency and fidelity based on an EIT-memory scheme through two different optical excitation channels. We also show that a nonlinear beam splitter that makes one optical soliton split into two ones can be obtained by switching on and off of the two control laser fields separately. In addition, the scheme can also be generalized to cases where one slow-light soliton can be split into three or more ones via a multichannel optical excitation process.

Before proceeding, we note that some studies have been carried out on soliton-related splitters in systems of photovoltaic materials [28–30], nonresonant Kerr media [31,32], liquid crystals [33,34], and Bose-Einstein condensates [35]. However, our paper is completely different from these studies. First, due to the resonant character of our system, the significant energy transfer via different quantum excitation channels plays a crucial role for the realization of the slow-light soliton splitters, which was absent in the systems considered in Refs. [28–35]. Second, the system suggested in our paper can be actively manipulated, and is easy to extend to cases with more optical excitation channels. Third, the slow-light soliton splitters obtained in our system can work at extremely low and even single-photon level, which is not viable in the systems used in Refs. [28–35]. The results reported in our paper open a route not only for active manipulation of nonlinear optical pulses but also for promising applications in optical and quantum information processing and transmission.

II. MODEL AND SLOW-LIGHT SOLITONS

A. Model

The system under consideration is a lifetime-broadened four-state atomic gas with a tripod-type level configuration, interacting resonantly with a weak pulsed probe laser field (with center wave number $k_p = \omega_p/c$, center angular frequency ω_p, and time duration τ_0 at the entrance of the medium) and two strong continuous-wave control laser fields (with wave numbers $k_{c1} = \omega_{c1}/c$ and $k_{c2} = \omega_{c2}/c$, and angular frequencies ω_{c1} and ω_{c2}, respectively). The probe field drives the transition $|1\rangle \leftrightarrow |0\rangle$, and the two control fields

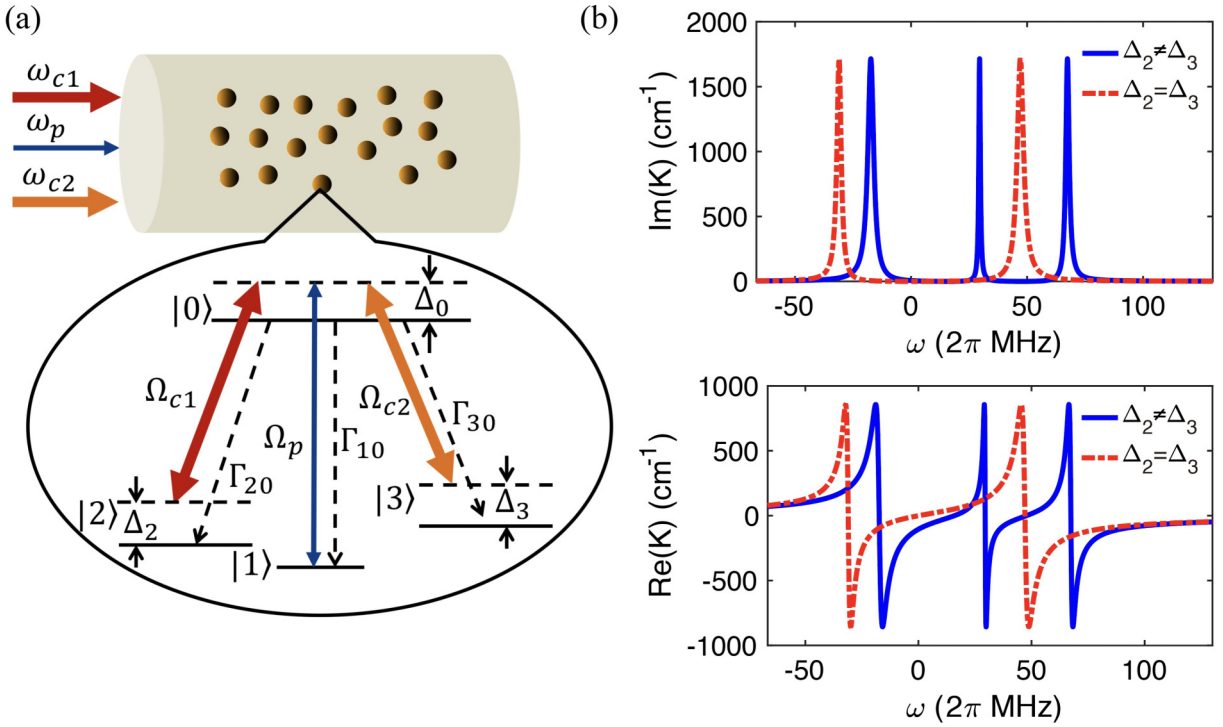

FIG. 1. (a) Atomic gas (brown dots) couples with a pulsed probe laser field (with center angular frequency ω_p and half Rabi frequency Ω_p) and two continuous-wave control laser fields [with angular frequencies ω_{c1} (half Rabi frequency Ω_{c1}) and ω_{c2} (half Rabi frequency Ω_{c2}), respectively]. Inset: Energy-level diagram and excitation scheme of the atomic gas with a tripod-type level configuration. Γ_{10} (Γ_{20}, Γ_{30}) is the decay rate from $|0\rangle$ to $|1\rangle$ ($|0\rangle$ to $|2\rangle$, $|0\rangle$ to $|3\rangle$); Δ_0 (Δ_2 and Δ_3) is one-photon (two-photon) detuning. (b) The imaginary part Im(K) (K is the linear dispersion relation of the system) as a function of ω, for $\Delta_2 \neq \Delta_3$ (solid blue line, which displays two transparency windows), and for $\Delta_2 = \Delta_3$ (dashed red line, which displays only one transparency window). The lower half part of the panel is the real part Re(K), for $\Delta_2 \neq \Delta_3$ (solid blue line), and for $\Delta_2 = \Delta_3$ (dashed red line).

drive, respectively, the transitions $|2\rangle \leftrightarrow |0\rangle$ and $|3\rangle \leftrightarrow |0\rangle$ [see Fig. 1(a)]. The total electric field in the system can be expressed as $\mathbf{E} = \mathbf{E}_p + \mathbf{E}_{c1} + \mathbf{E}_{c2} = \sum_{l=p,c1,c2} \mathbf{e}_l \mathcal{E}_l \exp[i(k_l z - \omega_l t)] + \text{c.c.}$, where $\mathbf{e}_l$ ($\mathcal{E}_l$) is the unit polarization vector (envelope) of the electric field $\mathbf{E}_l$. For simplicity, we have assumed that all laser fields propagate along the z direction.

The Hamiltonian of the system in the interaction picture reads

$$H_{\text{int}} = -\hbar\left(\sum_{j=0}^{3} \Delta_j |j\rangle\langle j| + \Omega_p |0\rangle\langle 1| + \Omega_{c1}|0\rangle\langle 2| + \Omega_{c2}|0\rangle\langle 3| + \text{H.c.}\right), \tag{1}$$

where $\Delta_1 = 0$, $\Delta_0 = \omega_p - (E_0 - E_1)/\hbar$ (one-photon detuning), $\Delta_2 = \omega_p - \omega_{c1} - (E_2 - E_1)/\hbar$, and $\Delta_3 = \omega_p - \omega_{c2} - (E_3 - E_1)/\hbar$ (two-photon detunings); E_j ($j = 0, 1, 2, 3$) is the energy eigenvalue of the atomic state $|j\rangle$; $\Omega_p = (\mathbf{e}_p \cdot \mathbf{p}_{10})\mathcal{E}_p/\hbar$, $\Omega_{c1} = (\mathbf{e}_{c1} \cdot \mathbf{p}_{20})\mathcal{E}_{c1}/\hbar$, and $\Omega_{c2} = (\mathbf{e}_{c2} \cdot \mathbf{p}_{30})\mathcal{E}_{c2}/\hbar$ are, respectively, the half Rabi frequencies of the probe and the two control fields; $\mathbf{p}_{ij}$ is the electric dipole matrix element associated with levels $|i\rangle$ and $|j\rangle$, with $\mathbf{e}_p$ ($\mathcal{E}_p$), $\mathbf{e}_{c1}$ ($\mathcal{E}_{c1}$), and $\mathbf{e}_{c2}$ ($\mathcal{E}_{c2}$), respectively, the polarization unit vectors (envelopes) of the probe and two control fields.

The atomic dynamics is described by a 4×4 density matrix σ, obeying the optical Bloch equation

$$\frac{\partial \sigma}{\partial t} = -\frac{i}{\hbar}[H_{\text{int}}, \sigma] - \Gamma[\sigma], \tag{2}$$

where Γ is a relaxation matrix characterizing the spontaneous emission and dephasing in the system [36]. The explicit form of Eq. (2) is presented in Appendix A.

The evolution of the probe field $\mathbf{E}_p$ is governed by the Maxwell equation $\nabla^2 \mathbf{E}_p - (1/c^2)\partial^2 \mathbf{E}_p/\partial t^2 = (1/\varepsilon_0 c^2)\partial^2 \mathbf{P}_p/\partial t^2$, where $\mathbf{P}_p = \mathcal{N}_a\{\mathbf{p}_{10}\sigma_{01}\exp[i(k_p z - \omega_p t)] + \text{c.c.}\}$ is the electric polarization intensity induced by the probe field, with $\mathcal{N}_a$ the atomic density. Under slowly varying envelope approximation, the Maxwell equation is reduced to

$$i\left(\frac{\partial}{\partial z} + \frac{1}{c}\frac{\partial}{\partial t}\right)\Omega_p + \kappa_{10}\sigma_{01} = 0, \tag{3}$$

where $\kappa_{10} = \mathcal{N}_a \omega_p |\mathbf{p}_{10}|^2/(2\varepsilon_0 c\hbar)$ is the coupling coefficient describing the interaction between the light field and atoms.

Notice that in the derivation of the above Maxwell-Bloch (MB) Eqs. (2) and (3), we have made the following assumptions.

(i) The probe pulse has a large transverse size so that the diffraction effect [i.e., the term proportional to $(\partial^2/\partial x^2 + \partial^2/\partial y^2)\Omega_p$] can be neglected.

(ii) Compared with the probe field, the two control fields are strong, so that their amplitudes ($\mathcal{E}_{c1}$ and $\mathcal{E}_{c2}$) can be undepleted during the evolution of the probe field. However, when considering the storage and retrieval of the probe field (see the next section), $\mathcal{E}_{c1}$ and $\mathcal{E}_{c2}$ (hence Ω_{c1} and Ω_{c2}) will be assumed to be varied adiabatically in time.

(iii) The atomic gas is cold and dilute, thereby the Doppler effect is negligible and the interaction between atoms can be described by the dephasing parameter $\gamma_{jl}^{\rm dep}$ (see Appendix A).

Note that the model mentioned above may be realized in realistic experiments. One example is an ultracold ^{87}Rb atomic gas [37], with the energy levels selected to be $|1\rangle = |5\,^2S_{1/2}, F = 1, m_F = -1\rangle$, $|2\rangle = |5\,^2S_{1/2}, F = 2, m_F = -1\rangle$, $|3\rangle = |5\,^2S_{1/2}, F = 2, m_F = 1\rangle$, and $|0\rangle = |5\,^2P_{1/2}, F = 1, m_F = 0\rangle$, which gives $|\mathbf{p}_{10}| \simeq |\mathbf{p}_{20}| \simeq |\mathbf{p}_{30}| = 2.54 \times 10^{-27}$ C cm. If the atomic density is chosen as $\mathcal{N}_a = 1.1 \times 10^{12}$ cm^{-3}, κ_{10} takes the value of 3.0×10^{10} cm^{-1} s^{-1}. This set of parameters will be used in the analysis and calculation given below.

B. Slow-light solitons

We start to consider the propagation of a linear probe pulse in the system. We assume that the two control fields are applied first and hence all the atoms are prepared in the ground state $|1\rangle$. When a weak probe pulse is present, the system undergoes a linear evolution. In this case, the MB Eqs. (2) and (3) admit the solution for Ω_p with the form $F\exp[i(Kz - \omega t)]$ [38], where F is a constant and K is the linear dispersion relation

$$K(\omega) = \frac{\omega}{c} - \frac{\kappa_{01}(\omega + d_{21})(\omega + d_{31})}{D}, \tag{4}$$

with $D = (\omega + d_{01})(\omega + d_{21})(\omega + d_{31}) - |\Omega_{c1}|^2(\omega + d_{31}) - |\Omega_{c2}|^2(\omega + d_{21})$. Shown in Fig. 1(b) is the imaginary part [i.e., Im(K)] and the real part [i.e., Re(K)] of K as functions of ω. The solid blue line and dashed red line in the figure are for $(\Delta_2, \Delta_3) = (-2\pi \times 15.9, -2\pi \times 47.7)$ and $(-2\pi \times 0.16, -2\pi \times 0.16)$ MHz, respectively. The other parameters are $\Delta_0 = -2\pi \times 15.9$ MHz, $\gamma_{01} = 2\pi \times 2.8$ MHz, $\gamma_{21} = 2\pi \times 8$ Hz, and $\gamma_{31} = 2\pi \times 15.9$ Hz. We see that when $\Delta_2 \neq \Delta_3$ the system displays a double EIT with two transparency windows; however, if $\Delta_2 = \Delta_3$, the double EIT is degenerated into a single EIT with only one transparency window. The reason for the occurrence of such degeneration is due to the symmetry of the tripod level configuration for $\Delta_2 = \Delta_3$. With such symmetry, the system is largely simplified, which will be considered in the discussion below.

EIT has been widely used for nearly free propagation of linear optical pulses in multistate quantum systems [25–27]. Yet, linear optical pulses in EIT-based systems generally experience serious deformation. The physical reason for the deformation is that in such systems the optical pulses interact with atoms (or other quantum emitters) resonantly and hence a significant dispersion is unavoidable for long-distance propagation. Thus it is necessary to find a way to suppress the dispersion and hence to obtain optical pulses that are robust during propagation. It has been shown in recent years that stable optical pulses are indeed possible if EIT-based systems work in a weak nonlinear region [39–41]. We now demonstrate that stable slow-light solitons are also possible in the present tripod system.

A weak nonlinear probe pulse in the system still has the form $\Omega_p = F\exp[i(Kz - \omega t)]$, but F is now an envelope function modulated slowly in both time and space. By exploiting a perturbation expansion with multiple scales developed in Ref. [40], the nonlinear envelope equation describing the evolution of F can be derived based on the MB Eqs. (2) and (3), which reads

$$i\frac{\partial}{\partial z}F - \frac{1}{2}K_2\frac{\partial^2}{\partial \tau^2}F + W|F|^2Fe^{-2\alpha z} = 0, \tag{5}$$

where $\tau = t - z/V_g$ [$V_g \equiv (\partial K/\partial\omega)^{-1}$ is the group velocity of the probe pulse], $\alpha = \mathrm{Im}(K)$ is an absorption coefficient, $K_2 = \partial^2 K/\partial\omega^2$ is a coefficient describing group-velocity dispersion, and W is a coefficient describing self-phase modulation. The detailed derivation of the nonlinear Schrödinger Eq. (5) and the explicit expressions of W and solutions up to the third order of the perturbation expansion have been presented in Appendix B.

If α is small, and the imaginary parts of K_2 and W are smaller compared with their corresponding real parts, Eq. (5) has the following soliton solution:

$$\Omega_p = \frac{1}{\tau_0}\sqrt{\frac{|\tilde{K}_2|}{\tilde{W}}}\,\mathrm{sech}\left[\frac{1}{\tau_0}\left(t - \frac{z}{\tilde{V}_g}\right)\right]\exp\left[i\left(\tilde{K}_0 - \frac{1}{2L_{\rm D}}\right)z\right], \tag{6}$$

for $\mathrm{sgn}(\tilde{K}_2) = -1$. Here $K_0 \equiv K|_{\omega=0}$; the tilde symbols over K_0, K_2, W, and V_g represent their corresponding real parts; $L_{\rm D} \equiv \tau_0^2/|\tilde{K}_2|$ is the typical dispersion length of the system.

To check that (6) is indeed a physical solution of the system, we take the realistic system parameters $\Omega_{c1} = 2\pi \times 27.1$ MHz, $\Omega_{c2} = 2\pi \times 27.1$ MHz, $\Delta_0 = -2\pi \times 15.9$ MHz, $\Delta_2 = \Delta_3 = -2\pi \times 1.9$ MHz, $\tau_0 = 5.0 \times 10^{-8}$ s, $\gamma_{21} = 2\pi \times 8.0$ Hz, $\gamma_{31} = 2\pi \times 15.9$ Hz, $\gamma_{01} = 2\pi \times 2.5$ MHz, $\omega_p = 2.37 \times 10^{15}$ Hz. Then we obtain $\alpha = 0.02$, $K_2 = (-2.4 + 0.3i) \times 10^{-15}$ cm^{-1} s^2, and $W = (3.5 - 0.02i) \times 10^{-16}$ cm^{-1} s^2. We see that α and the imaginary parts of K_2 and W are indeed small. The physical reason is that, under the EIT condition, the absorption of the system is largely suppressed by the EIT effect induced by the control fields, which guarantees the validity of the soliton solution given by (6). For more detailed discussion on the slow-light soliton and its stable propagation, see Appendix B.

Based on the parameters given above, we obtain the propagation velocity of the soliton:

$$\tilde{V}_g \simeq 6.14 \times 10^{-5}c, \tag{7}$$

which is much smaller than the light speed c in vacuum, thereby (6) is a slow-light soliton. The maximum average power density $\bar{P}_{\rm max}$ of the slow-light soliton can be estimated by using Poynting's vector [40]. For the transverse radius of the probe pulse $R = 300\,\mu$m, we obtain

$$\bar{P}_{\rm max} \simeq 7.06 \times 10^{-9}\,\mathrm{W}, \tag{8}$$

which is very low. From results (7) and (8), we see that the optical soliton obtained in the present tripod system has ultraslow propagation velocity and ultralow generation power,

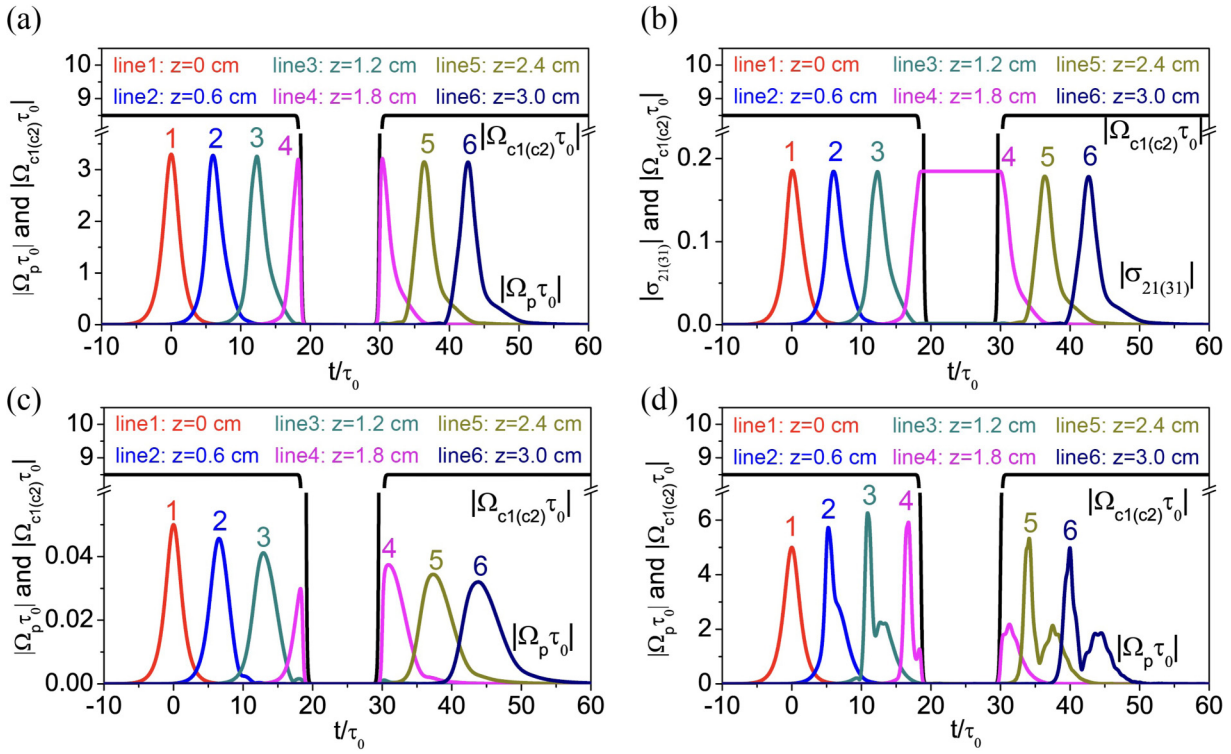

FIG. 2. Storage and retrieval of the slow-light pulses in the tripod system, for $\Delta_2 = \Delta_3 = -2\pi \times 1.9\,\mathrm{MHz}$ and $\Omega_{c1} = \Omega_{c2}$. (a) Evolution of $|\Omega_p\tau_0|$ in the soliton region as a function of t/τ_0 and z, with $\Omega_p(0,t)\tau_0 = 3.3\,\mathrm{sech}(t/\tau_0)$. Lines 1, 2, and 3 are, respectively, soliton profiles at $z = 0$, 0.6, and 1.2 cm (before storage); lines 4, 5, and 6 are, respectively, soliton profiles at $z = 1.8$, 2.4, and 3.0 cm (after the storage). The solid black line shows the switching off and on of the two control fields (they are overlapped completely) simultaneously. (b) Atomic coherences $|\sigma_{21}|$, $|\sigma_{31}|$ ($|\sigma_{21}| \approx |\sigma_{31}|$) in the soliton region [corresponding to (a)] before, during, and after the soliton storage. (c) $|\Omega_p\tau_0|$ in the dispersion-dominant region, with $\Omega_p(0,t)\tau_0 = 0.05\,\mathrm{sech}(t/\tau_0)$. (d) $|\Omega_p\tau_0|$ in the nonlinearity-dominant region, with $\Omega_p(0,t)\tau_0 = 5.0\,\mathrm{sech}(t/\tau_0)$.

which is very different from that obtained by using conventional optical media (e.g., fibers).

III. SLOW-LIGHT SOLITON BEAM SPLITTERS

EIT is one of the important methods for the storage and retrieval of optical pulses [25–27,42,43]. Recently, it has been shown that the EIT-based linear light memory can be extended to weak nonlinear optics regimes [44–46]. In the following, we show that the slow-light solitons of the tripod system obtained above can be used to build slow-light soliton beam splitters through the manipulation of the control fields in the system.

A. Storage and retrieval of slow-light solitons

Before the presentation on how to realize slow-light soliton beam splitters, we give a simple description for the storage and retrieval of optical solitons in the tripod system for the simple case where the two control fields are switched on and off simultaneously. The simultaneous switching on and off of the two control fields can be described by the following switching function:

$$\Omega_{cj} = \Omega_{cj0}\left[1 - \frac{1}{2}\tanh\left(\frac{t - T_{\mathrm{off}}^{j}}{T_s}\right) + \frac{1}{2}\tanh\left(\frac{t - T_{\mathrm{on}}^{j}}{T_s}\right)\right], \tag{9}$$

where Ω_{cj0} ($j = 1, 2$) is constant, T_s is the switching time, and T_{off}^{j} (T_{on}^{j}) is the time when switching off (on) Ω_{cj}. We take $\Omega_{c10} = \Omega_{c20} = 2\pi \times 27.1\,\mathrm{MHz}$, $T_{\mathrm{off}}^{1}/\tau_0 = T_{\mathrm{off}}^{2}/\tau_0 = 19.0$, $T_{\mathrm{on}}^{1}/\tau_0 = T_{\mathrm{on}}^{2}/\tau_0 = 30.0$, and $T_s/\tau_0 = 0.2$ (with $\tau_0 = 5.0 \times 10^{-8}\ \mathrm{s}^{-1}$), and exploit Runge-Kutta method to solve Eqs. (2) and (3).

Shown in Fig. 2(a) is the result of a numerical simulation on the storage and retrieval of the slow-light soliton for $\Delta_2 = \Delta_3 = -2\pi \times 1.9\,\mathrm{MHz}$, by taking $|\Omega_p\tau_0|$ as a function of t/τ_0 and z. Lines 1, 2, and 3 are, respectively, soliton profiles at the positions $z = 0$, 0.6, and 1.2 cm (before storage); lines 4, 5, and 6 are, respectively, soliton profiles at positions 1.8, 2.4, and 3.0 cm (after the storage). The solid black line in the figure shows the simultaneous switching off and on of the two control fields (i.e., $\Omega_{c1} = \Omega_{c2}$). The initial condition used in the simulation is $\Omega_p(0,t)\tau_0 = 3.3\,\mathrm{sech}(t/\tau_0)$; system parameters are $\Delta_0 = -2\pi \times 15.9\,\mathrm{MHz}$, $\gamma_{21} = 2\pi \times 8.0\,\mathrm{Hz}$, $\gamma_{31} = 2\pi \times 15.9\,\mathrm{Hz}$, $\gamma_{01} = 2\pi \times 2.5\,\mathrm{MHz}$. From the figure, we see that the soliton is very stable before the storage, and the retrieved soliton (after the storage) is also quite stable and has nearly the same wave shape as that before the storage. The physical reason of the shape preservation during the soliton generation process is due to the balance between the dispersion and the Kerr nonlinearity of the system. The approximated expression of the probe soliton during the storage and retrieval is presented in Appendix C1.

Figure 2(b) shows the result of atomic coherences $|\sigma_{21}|$ and $|\sigma_{31}|$ ($|\sigma_{21}| \approx |\sigma_{31}|$), as functions of t/τ_0 and z during the process of the storage and retrieval of the soliton. One sees that $|\sigma_{21}|$ and $|\sigma_{31}|$ are nonzero during the period when both control fields are switched off. Such result is a manifestation of the information transfer from the probe field to the atomic internal states during the storage, which can be understood through the stable propagation of the dark-state polaritons in the system [44–46].

The efficiency of the slow-light soliton memory can be characterized by [44–46]

$$\eta = \frac{\int_{-\infty}^{+\infty} \left|E_p^{\rm out}(t)\right|^2 dt}{\int_{-\infty}^{+\infty} \left|E_p^{\rm in}(t)\right|^2 dt}, \tag{10}$$

where $E_p^{\rm in}(t) = E_p^{\rm in}(z,t)|_{z=0}$ (the input soliton pulse) and $E_p^{\rm out}(t) = E_p^{\rm out}(z,t)|_{z=L_z}$ [the output (i.e., retrieved) soliton pulse], with L_z (=3.0 cm) the medium length. From Fig. 2(a) we obtain $\eta = 0.92$. The soliton memory efficiency will be increased if its storage time is shortened (or L_z is reduced).

The fidelity of the soliton memory can be described by the parameter ηJ^2, where J^2 describes the degree of coincidence of the wave shapes for the input and output solitons, defined by the overlap integral

$$J^2 = \frac{\left|\int_{-\infty}^{+\infty} E_p^{\rm out}(t) E_p^{\rm in}(t+\Delta T)dt\right|^2}{\int_{-\infty}^{+\infty} \left|E_p^{\rm out}(t)\right|^2 dt \int_{-\infty}^{+\infty} \left|E_p^{\rm in}(t+\Delta T)\right|^2 dt}, \tag{11}$$

where ΔT is the time interval between the peak of the input soliton pulse $E_p^{\rm in}$ and the peak of the output soliton pulse $E_p^{\rm out}$. From Fig. 2(a) we obtain $J^2 = 0.98$ and hence $\eta J^2 = 0.90$. Thus, the memory of the slow-light soliton in the tripod system has a nice quality due to the balance between the dispersion and nonlinearity in the system.

Plotted in Fig. 2(c) is the result for the optical pulse memory in a dispersion-dominant (i.e., linear) region, with $\Omega_p(0,t)\tau_0 = 0.05\,\mathrm{sech}(t/\tau_0)$. In this case, the dispersion length of the system $L_{\rm D} = 1.05$ cm is much smaller than the nonlinearity length $L_{\rm NL} = 719.0$ cm. From the figure we see that the optical pulse is broadened significantly before and after the storage, with the memory efficiency and fidelity given by $(\eta,\ \eta J^2) = (0.93,\ 0.75)$. Figure 2(d) shows the pulse memory in a nonlinearity-dominant (i.e., strong nonlinear) region, with $\Omega_p(0,t)\tau_0 = 5.0\,\mathrm{sech}(t/\tau_0)$. In this situation, the nonlinearity length $L_{\rm NL} = 0.36$ cm is much smaller than the dispersion length $L_{\rm D} = 1.05$ cm. We see that the optical pulse has a very large distortion before and after the storage, with $(\eta,\ \eta J^2) = (0.79,\ 0.60)$. Consequently, the optical pulse memory in these two regions has lower quality compared with that of the soliton region.

B. Slow-light soliton beam splitters through two optical excitation channels

We now turn to describe how to realize a slow-light soliton beam splitter in the system. Similar to linear beam splitters [22], the slow-light soliton beam splitter can be realized through an adiabatical switching off and on of the two control laser fields subsequently. The switching off and on of the two control fields can be described by the following switching functions:

$$\Omega_{c1} = \Omega_{c10}\left[\frac{1}{2} - \frac{1}{2}\sum_{i=1}^{2}\tanh\left(\frac{t-T_{{\rm off}_i}^1}{T_s}\right) + \frac{1}{2}\tanh\left(\frac{t-T_{\rm on_1}^1}{T_s}\right)\right], \tag{12a}$$

$$\Omega_{c2} = \Omega_{c20}\left[1 - \frac{1}{2}\tanh\left(\frac{t-T_{\rm off_1}^2}{T_s}\right) + \frac{1}{2}\tanh\left(\frac{t-T_{\rm on_1}^2}{T_s}\right)\right], \tag{12b}$$

where Ω_{cj0} ($j = 1, 2$) is constant, T_s is the switching time, and $T_{{\rm off}_i}^j$ ($T_{{\rm on}_i}^j$) is the ith switching off (switching on) of the control field Ω_{cj}. The timing sequence of the switching off and on of Ω_{cj} for obtaining a slow-light soliton beam splitter is shown in Fig. 3(a), with $T_{\rm off_1}^1 = T_{\rm off_1}^2 < T_{\rm on_1}^1 < T_{\rm off_2}^1 < T_{\rm on_1}^2$.

Figure 3(b) shows the result of a numerical simulation on how to obtain a slow-light soliton beam splitter by taking $|\Omega_p\tau_0|$ as a function of t/τ_0 and z (with $\tau_0 = 5.0\times10^{-8}$ s). The operation steps can be described as follows.

(1) A weak nonlinear probe pulse is incident at $z = 0$ with the waveform $\Omega_p(0,t)\tau_0 = 3.3\,\mathrm{sech}(t/\tau_0)$. A slow-light soliton forms via the balance between dispersion and Kerr nonlinearity, and propagates stably to $z = 0.6$ and 1.2 cm (corresponding times are $5.3\tau_0$ and $11.0\tau_0$), respectively. This is the soliton (the leftmost red pulses) before the storage.

(2) Both Ω_{c1} and Ω_{c2} are switched off at $t = T_{\rm off_1}^1 = T_{\rm off_1}^2 = 15\tau_0$; the (input) probe soliton is stored in the two atomic coherences σ_{21} and σ_{31} (which are not shown in the figure for saving space) simultaneously.

(3) By switching on Ω_{c1} at $t = T_{\rm on_1}^1 = 30\tau_0$ but keeping Ω_{c2} switched off, the atomic coherence σ_{21} is converted back into the probe pulse, and hence a new soliton (called soliton 1) is retrieved. The figure (the middle blue pulses) shows the propagation of the soliton to $z = 2.4$, 2.7, and 3.0 cm (corresponding times are $t = 44.9\tau_0$, $50.4\tau_0$, and $56.1\tau_0$), respectively.

(4) At $t = T_{\rm off_2}^1 = 80\tau_0$, Ω_{c1} is switched off; after time $20\tau_0$, Ω_{c2} is switched on at $t = T_{\rm on_1}^2 = 100\tau_0$. The atomic coherence σ_{31} is converted back into the probe pulse, and thus another new soliton (called soliton 2) is retrieved. The figure (the rightmost yellow pulses) shows the propagation of the soliton 2 to $z = 2.4$, 2.7, and 3.0 cm (corresponding times are $t = 114.9\tau_0$, $120.4\tau_0$, and $126.0\tau_0$), respectively.

In the simulation, the other system parameters are chosen to be $\Delta_0 = -2\pi\times15.9$ MHz, $\Delta_2 = \Delta_3 = -2\pi\times1.9$ MHz, $\gamma_{21} = 2\pi\times8.0$ Hz, $\gamma_{31} = 2\pi\times15.9$ Hz, $\gamma_{01} = 2\pi\times2.5$ MHz, and $\Omega_{c10} = \Omega_{c20} = 2\pi\times28.6$ MHz, $T_s = 0.2\tau_0$. From the figure, we see that the input probe soliton can indeed be stored and partially retrieved by switching on both control fields subsequently, behaving like a soliton beam splitter. The retrieved soliton 1 and soliton 2 are very similar to the stored one due to the balance between the dispersion and Kerr nonlinearity, except for a smaller amplitude and a wider temporal width compared with the input soliton. Note that the amplitude of each retrieved pulse has the same magnitude of order as that of the stored soliton, thereby two retrieved pulses are still solitons of the system. The approximated expression

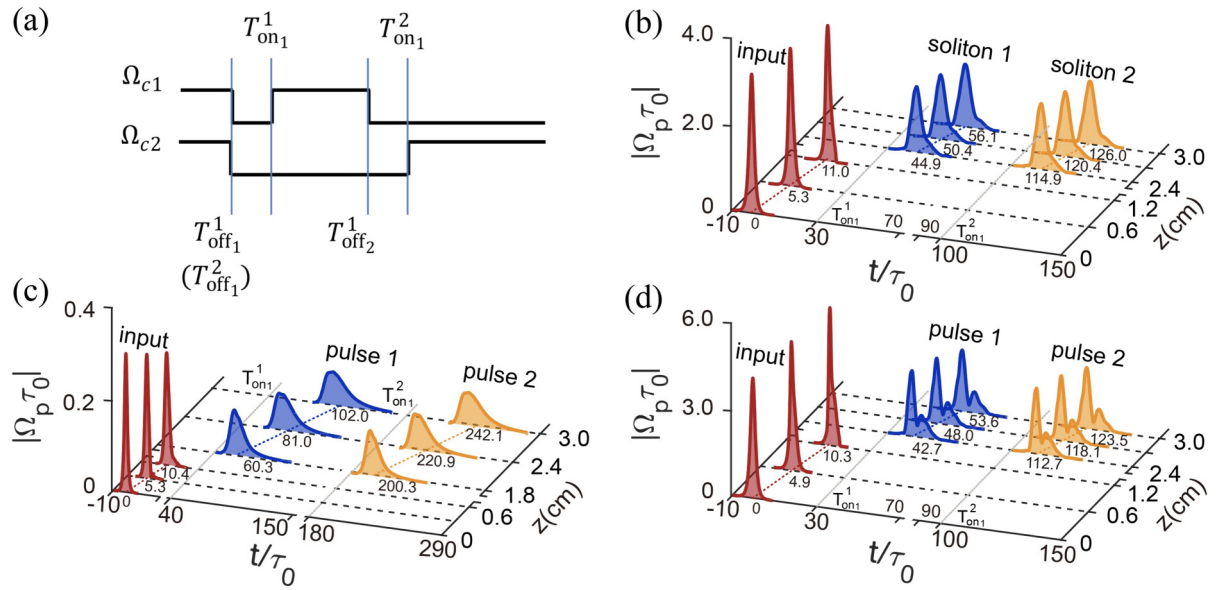

FIG. 3. Slow-light soliton beam splitters through two optical excitation channels. (a) Timing sequence of the switching on and off of the control fields Ω_{c1} and Ω_{c2} for obtaining the slow-light soliton beam splitter, with $T^j_{\text{off}_i}$ ($T^j_{\text{on}_i}$) the ith time of switching off and on of the control field Ω_{cj} ($j = 1, 2$). (b) Soliton splitting by taking $|\Omega_p\tau_0|$ as a function of t/τ_0 ($\tau_0 = 5.0 \times 10^{-8}$ s) and z. The leftmost three red pulses are for the probe soliton before the storage when it propagates to $z = 0.6$ and 1.2 cm (corresponding times are $t = 5.3\tau_0$ and $11.0\tau_0$), respectively. The middle three blue pulses are for the retrieved new soliton (soliton 1) when it propagates to $z = 2.4$, 2.7, and 3.0 cm (corresponding times are $t = 44.9\tau_0$, $50.4\tau_0$, and $56.1\tau_0$), respectively. The rightmost three yellow pulses are for another retrieved new soliton (soliton 2) when it propagates to $z = 2.4$, 2.7, and 3.0 cm (corresponding times are $t = 114.9\tau_0$, $120.4\tau_0$, and $126.0\tau_0$), respectively. For more details, see the text. (c) Similar to panel (b) but for the pulse splitting in a dispersion-dominant region. (d) Similar to panel (b) but for the pulse splitting in a nonlinearity-dominant region.

of the probe pulse during the soliton splitting is presented in Appendix C2.

For comparison, Fig. 3(c) [Fig. 3(d)] shows the result of numerical simulations on the pulse splitting in a dispersion-dominant (nonlinearity-dominant) region, with the input pulse given by $\Omega_p(0, t)\tau_0 = 0.3\,\text{sech}(t/\tau_0)$ [$\Omega_p(0, t)\tau_0 = 4.5\,\text{sech}(t/\tau_0)$] and all other parameters the same as those used in panel (b) but $\tau_0 = 2.5 \times 10^{-8}$ s ($\tau_0 = 5.0 \times 10^{-8}$ s). We see that, though one can get pulse storage and splitting, the retrieved pulses have large deformation compared with the input one. The reason is that in both the dispersion- and nonlinearity-dominant regions there is no balance between the dispersion and Kerr nonlinearity, and thereby a spreading or distortion of the pulse is unavoidable in the processes of the storage and splitting.

We now give a simple explanation for the memory and splitting of the slow-light soliton described above, based on the Bloch Eq. (2) (its explicit expression is given in Appendix A). Since for a weak probe pulse $d_{21}\sigma_{21}$, $d_{31}\sigma_{31}$, $\Omega_p\sigma_{02}$, and $\Omega_p\sigma_{03}$ are small, from Eqs. (A2a) and (A2b) one has

$$\sigma_{01} = -i\frac{1}{|\Omega_{c1}|^2 + |\Omega_{c2}|^2}\left(\Omega_{c1}\frac{\partial\sigma_{21}}{\partial t} + \Omega_{c2}\frac{\partial\sigma_{31}}{\partial t}\right). \quad (13)$$

Substituting Eq. (13) into Eq. (A2d) and using $\sigma_{11} \approx 1$ and $\sigma_{00} \approx 0$, we obtain

$$\Omega_{c1}\sigma_{21} + \Omega_{c2}\sigma_{31} = -\Omega_p - \frac{1}{|\Omega_{c1}|^2 + |\Omega_{c2}|^2}\left(\frac{\partial}{\partial t} + id_{01}\right)\left(\Omega_{c1}\frac{\partial\sigma_{21}}{\partial t} + \Omega_{c2}\frac{\partial\sigma_{31}}{\partial t}\right) \simeq -\Omega_p. \quad (14)$$

Equation (14) can be rewritten as the form $\sigma_{21} + (\Omega_{c2}/\Omega_{c1})\sigma_{31} \simeq -(\Omega_p/\Omega_{c1})$. Thereby, σ_{21} and σ_{31} may acquire nonzero values if the rations Ω_{c2}/Ω_{c1} and Ω_p/Ω_{c1} remain finite constant values, though during the storage Ω_{c1} and Ω_{c2} are switched off and Ω_p approaches zero; in the retrieval process, the probe pulse can be recovered when Ω_{c1} and Ω_{c2} are switched on again. This can also be understood by the existence of the two dark-state polaritons in the system, which read [6,8].

$$\Psi = \cos\theta\Omega_p - g\sqrt{\mathcal{N}_a}\sin\theta[\cos\phi\exp(i\chi_{c1})\sigma_{21} + \sin\phi\exp(i\chi_{c2})\sigma_{31}], \quad (15a)$$

$$Z = \sin\phi e^{i\chi_{c1}}\sigma_{21} - \cos\phi e^{i\chi_{c2}}\sigma_{31}, \quad (15b)$$

where $g^2 = |\mathbf{p}_{01}|^2\omega_p/(2\epsilon_0\hbar)$, $\cos\phi = |\Omega_{c1}|/|\Omega_c|$, $\sin\phi = |\Omega_{c2}|/|\Omega_c|$, $\sin\theta = g\sqrt{\mathcal{N}_a}/\sqrt{|\Omega_c|^2 + g^2\mathcal{N}_a}$, $\cos\theta = |\Omega_c|/\sqrt{|\Omega_c|^2 + g^2\mathcal{N}_a}$, $\chi_{cj} = -i\ln(\Omega_{cj}/|\Omega_{cj}|)$ ($j = 1, 2$),

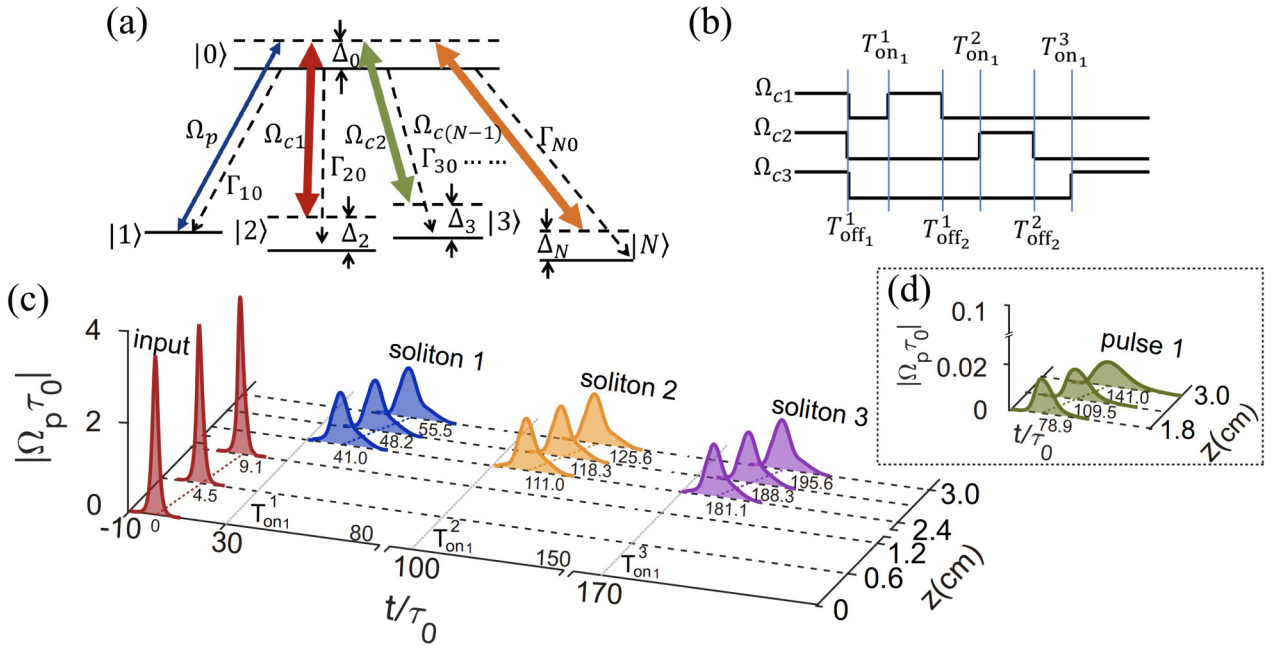

FIG. 4. Slow-light soliton beam splitter via multiple optical excitation channels. (a) Excitation scheme of the N-pod system. (b) Timing sequence for adiabatically manipulating the three control fields Ω_{c1}, Ω_{c2}, and Ω_{c3} in a quadripod system, for obtaining a slow-light soliton beam splitter via three optical excitation channels. (c) Numerical result on the splitting of the slow-light soliton in the quadripod system, by taking $|\Omega_p\tau_0|$ as a function of t/τ_0 and z. (d) When the system works in a dispersion-dominant region, the retrieved (linear) optical pulse deforms significantly. See the text for more details.

with $|\Omega_c| = \sqrt{|\Omega_{c1}|^2 + |\Omega_{c2}|^2}$. Since the nonlinear effect under consideration is weak, and during the soliton memory process both Ω_{c1} and Ω_{c2} are changed adiabatically, it can be shown that the dark-state polariton functions (15a) and (15b) satisfy equations $\partial\Psi/\partial t + c\cos^2\theta\partial\Psi/\partial z \approx 0$ and $\partial Z/\partial t \approx 0$. This means that during the soliton memory process the information of the probe soliton Ω_p is transferred into the two atomic coherences σ_{21} and σ_{31}, and vice versa, as shown in Fig. 2(b). This explanation applies also for the storage and retrieval processes in the soliton splitting illustrated in Fig. 3. For expressions of the probe pulse during the soliton splitting, see Appendix C2.

C. Slow-light soliton beam splitters through multiple optical excitation channels

The scheme proposed above can be generalized to systems with more optical excitation channels. Shown in Fig. 4(a) are the level diagram and excitation scheme of a N-pod system, where one probe field (with half Rabi frequency Ω_p) drives transition $|1\rangle$ to $|0\rangle$ and $N-1$ control fields (with half Rabi frequencies Ω_{cj}) drive transitions $|j\rangle$ to $|0\rangle$ ($j = 2, \cdots, N$). Γ_{j0} is the decay rate from $|0\rangle$ to $|j\rangle$ and Δ_j ($j \neq 1$) is the two-photon detuning ($j = 1, \cdots, N$). To realize a slow-light soliton beam splitter in such system, the control fields Ω_{cj} ($j = 1, \cdots, N-1$) must be adiabatically manipulated in a suitable way. For simplicity, here we consider only the case of a quadripod system, with the timing sequence of the three control fields Ω_{c1}, Ω_{c2}, and Ω_{c3} shown in Fig. 4(b). Plotted in Fig. 4(c) is the result of a numerical simulation for how to obtain the slow-light soliton beam splitter via three optical excitation channels, with operation steps described as follows.

(1) Initially (before the storage), the three control fields are switched on simultaneously, so a probe soliton forms in the system. The leftmost three red pulses in Fig. 4(c) are the soliton profile when it propagates to $z = 0$, 0.6, and 1.2 cm (corresponding times are $t = 0$, $4.5\tau_0$, and $9.1\tau_0$), respectively.

(2) At the time $T^1_{\text{off}_1}$, the three control fields are switched off simultaneously. When Ω_{c1} is switched on again at the time slot $T^1_{\text{on}_1} < t < T^1_{\text{off}_2}$ (but Ω_{c2} and Ω_{c3} remain switched off), a new soliton (called soliton 1) is retrieved from the atomic coherence σ_{21}. Blue pulses in Fig. 4(c) are for the retrieved soliton 1 when it propagates to $z = 2.4$, 2.7, and 3.0 cm (corresponding times are $t = 41.0\tau_0$, $48.2\tau_0$, and $55.5\tau_0$), respectively.

(3) At the time $T^1_{\text{off}_2}$, we switch off Ω_{c1} and hence the soliton 1 disappears. Then, at the time $T^2_{\text{on}_1}$, Ω_{c2} is switched on again in the time slot $T^2_{\text{on}_1} < t < T^2_{\text{off}_2}$ (but Ω_{c1} and Ω_{c3} remain switched off), and another new soliton (called soliton 2) is retrieved from the atomic coherence σ_{31}. Yellow pulses in Fig. 4(c) are for the retrieved soliton 2 when it propagates to $z = 2.4$, 2.7, and 3.0 cm (corresponding times are $t = 111.0\tau_0$, $118.3\tau_0$, and $125.6\tau_0$), respectively.

(4) At the time $T^2_{\text{off}_2}$, we switch off Ω_{c2} and hence the soliton 2 also disappears. Then, at the time $T^3_{\text{on}_1}$, Ω_{c3} is switched on again (but Ω_{c1} and Ω_{c2} remain switched off), and a third new soliton (called soliton 3) is retrieved from the atomic coherence σ_{41}. Purple pulses in the figure are for the retrieved soliton 3 when it propagates to $z = 2.4$, 2.7, and 3.0 cm (corresponding times are $t = 181.1\tau_0$, $188.3\tau_0$, and $195.6\tau_0$), respectively.

In the simulation, we use the parameters $\tau_0 = 5.0 \times 10^{-8}$ s, $T^1_{\text{off}_1} = 25\tau_0$, $T^1_{\text{on}_1} = 30\tau_0$, $T^1_{\text{off}_2} = 80\tau_0$, $T^2_{\text{on}_1} = 100\tau_0$,

$T^2_{\text{off}_2} = 150\tau_0$, and $T^3_{\text{on}_1} = 170\tau_0$. The probe pulse at the entrance of the medium is $\Omega_p(0,t)\tau_0 = 3.5\,\text{sech}(t/\tau_0)$. We see that the slow-light soliton beam splitter can be indeed realized through three optical excitation channels through adiabatically manipulating the three control fields. We stress that the retrieved pulses are indeed solitons because there is a balance between the dispersion and nonlinearity in the system, thereby these retrieved pulses are very stable during propagation. For comparison, panel (d) shows a retrieved linear pulse with $\tau_0 = 2.5 \times 10^{-8}$ s (which has been stored in the system first by switching off the three control fields simultaneously) when Ω_{c1} is switched on again. Here the probe pulse at the entrance of the medium is $\Omega_p(0,t)\tau_0 = 0.1\,\text{sech}(t/\tau_0)$. One sees that the retrieved pulse (green profiles) is deformed significantly during propagation since in this case the system works in a dispersion-dominant region.

IV. SUMMARY

Note that a retrieval of multiple optical pulses stored in a three-level Λ-type atomic system was considered in an interesting work by Reim *et al*. [48]. We stress that our work is different from that reported in Ref. [48]. First, the storage and retrieval of the optical pulses in our work are based on a scheme of EIT memory, while Ref. [48] is based on a Raman memory. Second, what we have investigated here is for the storage and retrieval of nonlinear (soliton) optical pulses, while Ref. [48] is for those of linear optical pulses. Third, the slow-light soliton beam splitter is hard to realize by using the three-level Λ-type atomic system with the control field consisting of several narrow subpulses in the retrieval period, proposed in Ref. [48]. To demonstrate this, based on a three-level Λ-type memory scheme we have carried out a numerical simulation on the single-pulse storage and multiple-pulse retrieval by using the retrieval technique described in Ref. [48]. We found that, though a beam splitting for the input narrow probe pulse may be obtained and the retrieved probe subpulses can be shaped by engineering the control field, a slow-light soliton beam splitter is not possible to realize with such scheme. The physical reason is that with such scheme the retrieved probe subpulses are unstable during propagation due to the loss and the unbalanced nonlinearity and (large) dispersion that cannot be avoided in the multiple-pulse retrieval process. In contrast, in our four-level tripod-type scheme with multiple excitation channels illustrated above, during the retrieval process the loss is small and the dispersion (also small) is well balanced by the weak nonlinearity of the system. Thus the optical solitons obtained in our scheme are quite stable during the processes of the propagation, storage, and retrieval, which makes the high performance realization of the soliton beam splitters possible.

In conclusion, in this paper we have proposed a scheme for realizing slow-light soliton beam splitters with a tripod-type four-state atomic system. By using the method of multiple scales, we have derived the nonlinear envelope equation governing the evolution of the probe pulse. We have shown that optical solitons with ultraslow propagation velocity and ultralow generation power can be produced in the system via EIT. We have also shown that these slow-light solitons can be stored and retrieved with high efficiency and fidelity through two different photonic channels. Based on this, a slow-light soliton beam splitter that splits one optical soliton into two ones can be implemented through the switching off and on of the two control laser fields subsequently. Furthermore, the possibility of the soliton beam splitter that splits one optical soliton into three or more ones via multiphotonic channels has also been illustrated.

The results reported here can be generalized to high-dimensional nonlinear optical pulses with orbital angular momenta, surface polaritons in metal-metamaterial interfaces, excitons in semiconductor quantum wells and dots, etc. Hence our paper opens a route not only for active manipulation of nonlinear optical pulses in multistate quantum systems but also for potential applications in optical information processing and transmission.

ACKNOWLEDGMENTS

This work was supported by the National Natural Science Foundation of China under Grants No. 11475063 and No. 11474099.

APPENDIX A: BLOCH EQUATION FOR THE DENSITY MATRIX

The explicit form of the Bloch Eq. (2) reads [36]

$$i\frac{\partial}{\partial t}\sigma_{11} - i\Gamma_{10}\sigma_{00} + \Omega_p^*\sigma_{01} - \Omega_p\sigma_{01}^* = 0, \tag{A1a}$$

$$i\frac{\partial}{\partial t}\sigma_{22} - i\Gamma_{20}\sigma_{00} + \Omega_{c1}^*\sigma_{02} - \Omega_{c1}\sigma_{02}^* = 0, \tag{A1b}$$

$$i\frac{\partial}{\partial t}\sigma_{33} - i\Gamma_{30}\sigma_{00} + \Omega_{c2}^*\sigma_{03} - \Omega_{c2}\sigma_{03}^* = 0, \tag{A1c}$$

$$i\frac{\partial}{\partial t}\sigma_{00} + i\Gamma_0\sigma_{00} - \Omega_p^*\sigma_{01} + \Omega_p\sigma_{01}^* - \Omega_{c1}^*\sigma_{02} + \Omega_{c1}\sigma_{02}^* - \Omega_{c2}^*\sigma_{03} + \Omega_{c2}\sigma_{03}^* = 0, \tag{A1d}$$

for diagonal matrix elements, and

$$\left(i\frac{\partial}{\partial t} + d_{21}\right)\sigma_{21} - \Omega_p\sigma_{02}^* + \Omega_{c1}^*\sigma_{01} = 0, \tag{A2a}$$

$$\left(i\frac{\partial}{\partial t} + d_{31}\right)\sigma_{31} - \Omega_p\sigma_{03}^* + \Omega_{c2}^*\sigma_{01} = 0, \tag{A2b}$$

$$\left(i\frac{\partial}{\partial t} + d_{32}\right)\sigma_{32} - \Omega_{c1}\sigma_{03}^* + \Omega_{c2}^*\sigma_{02} = 0, \tag{A2c}$$

$$\left(i\frac{\partial}{\partial t} + d_{01}\right)\sigma_{01} - \Omega_p(\sigma_{00} - \sigma_{11}) + \Omega_{c1}\sigma_{21} + \Omega_{c2}\sigma_{31} = 0, \tag{A2d}$$

$$\left(i\frac{\partial}{\partial t} + d_{02}\right)\sigma_{02} - \Omega_{c1}(\sigma_{00} - \sigma_{22}) + \Omega_p\sigma_{21}^* + \Omega_{c2}\sigma_{32} = 0, \tag{A2e}$$

$$\left(i\frac{\partial}{\partial t} + d_{03}\right)\sigma_{03} - \Omega_{c2}(\sigma_{00} - \sigma_{33}) + \Omega_p\sigma_{31}^* + \Omega_{c1}\sigma_{32}^* = 0, \tag{A2f}$$

for nondiagonal matrix elements, where $d_{jl} = \Delta_j - \Delta_l + i\gamma_{jl}$. Here $\gamma_{jl} = (\Gamma_j + \Gamma_l)/2 + \gamma_{jl}^{\text{dep}}$ is the decay rate of the

atomic coherence σ_{jl}, with $\Gamma_j = \sum_{E_l<E_j} \Gamma_{lj}$ the spontaneous-emission rate of the state $|j\rangle$ and $\gamma_{jl}^{\rm dep}$ the dephasing rate representing the loss of phase coherence between $|j\rangle$ and $|l\rangle$ contributed by atomic collisions and other incoherent processes [36].

APPENDIX B: DERIVATION OF THE NONLINEAR ENVELOPE EQUATION AND ITS SOLITON SOLUTION

To obtain the envelope equation governing the nonlinear evolution of the probe field based on the MB Eqs. (2) and (3), we take the asymptotic expansions [40,47]

$$\sigma_{jl} = \sigma_{jl}^{(0)} + \epsilon\sigma_{jl}^{(1)} + \epsilon^2\sigma_{jl}^{(2)} + \epsilon^3\sigma_{jl}^{(3)} + \cdots, \tag{B1a}$$

$$\Omega_p = \epsilon\Omega_p^{(1)} + \epsilon^2\Omega_p^{(2)} + \epsilon^3\Omega_p^{(3)} + \cdots, \tag{B1b}$$

with $\sigma_{jl}^{(0)} = \delta_{j0}\delta_{l0}$ the steady-state solution when the probe field is absent and ϵ the dimensionless small parameter characterizing the typical amplitude of the probe field. To have a divergence-free expansion that is valid for the nonlinear evolution of the system, all the components on the right-hand side of the expansion (B1) for σ_{jl} and Ω_p must be considered to be functions of the multiscale variables $z_l = \epsilon^l z$ ($l = 0, 1, 2$), $t_l = \epsilon^l t$ ($l = 0, 1$) [40,47]. Substituting such expansion to the MB Eqs. (2) and (3), we obtain a set of expansion equations which can be solved order by order.

At the first order of the expansion, we obtain the solution

$$\Omega_p^{(1)} = F\exp(i\theta), \tag{B2a}$$

$$\sigma_{21}^{(1)} = [\Omega_{c1}^*(\omega + d_{31})/D]F\exp(i\theta), \tag{B2b}$$

$$\sigma_{31}^{(1)} = [\Omega_{c2}^*(\omega + d_{21})/D]F\exp(i\theta), \tag{B2c}$$

$$\sigma_{01}^{(1)} = -[(\omega + d_{21})(\omega + d_{31})/D]F\exp(i\theta), \tag{B2d}$$

with all other $\sigma_{jl}^{(1)}$ zero. Here $\theta = K(\omega)z_0 - \omega t_0$ [38]; F is the envelope function of the slow variables z_1, z_2, and t_1; $K(\omega)$ is the linear dispersion relation [given by Eq. (4)]. The explicit expression of the quantity D can be found just below Eq. (4).

At the second order of the expansion, we obtain the envelope equation

$$i\left(\frac{\partial F}{\partial z_1} + \frac{1}{V_g}\frac{\partial F}{\partial t_1}\right) = 0, \tag{B3}$$

where $V_g \equiv (\partial K/\partial\omega)^{-1}$ is the group velocity of the probe pulse. Explicit expressions of the solution at this order are given by $\sigma_{j1}^{(2)} = a_{j1}^{(2)} i\frac{\partial}{\partial t_1}F\exp(i\theta)$ ($j = 0, 2, 3$), $\sigma_{02(03,32)}^{(2)} = a_{02(03,32)}^{(2)}|F|^2\exp(-2\bar{\alpha}z_2)$, and $\sigma_{jj}^{(2)} = a_{jj}^{(2)}|F|^2\exp(-2\bar{\alpha}z_2)$ ($j = 1, 2, 3, 0$), with

$$a_{01}^{(2)} = \frac{1}{\kappa_{01}}\left(\frac{1}{V_g} - \frac{1}{c}\right), \tag{B4a}$$

$$a_{21}^{(2)} = -\frac{\Omega_{c1}^*}{D^2}(\omega + d_{31})^2(2\omega + d_{01} + d_{21}) + \frac{\Omega_{c1}^*}{D^2}|\Omega_{c2}|^2(d_{31} - d_{21}), \tag{B4b}$$

$$a_{31}^{(2)} = -\frac{\Omega_{c2}^*}{D^2}(\omega + d_{21})^2(2\omega + d_{01} + d_{31}) + \frac{\Omega_{c2}^*}{D^2}|\Omega_{c1}|^2(d_{21} - d_{31}), \tag{B4c}$$

$$a_{22}^{(2)} = \frac{-\Gamma_{30}X + \Gamma_{10}(B - B^*)}{\Gamma_{10}(A - A^*)}, \tag{B4d}$$

$$a_{33}^{(2)} = \frac{Q + i\Gamma_{10}|\Omega_{c1}|^2(N^* - N)a_{22}^{(2)}}{i\Gamma_{10}P}, \tag{B4e}$$

$$a_{11}^{(2)} = \frac{X - i\Gamma_{10}\left(a_{22}^{(2)} + a_{33}^{(2)}\right)}{i\Gamma_{10}}, \tag{B4f}$$

$$a_{02}^{(2)} = \frac{M\left[\Omega_{c2}^*\left(\frac{1}{i\Gamma_{10}}X + a_{33}^{(2)}\right) + a_{31}^{(1)}\right] - a_{21}^{*(1)} - \Omega_{c1}\left(\frac{1}{i\Gamma_{10}}X + a_{22}^{(2)}\right)}{N}, \tag{B4g}$$

$$a_{03}^{(2)} = -\frac{M^*d_{32}^*}{\Omega_{c1}\Omega_{c2}}\left[\Omega_{c2}\left(\frac{1}{i\Gamma_{10}}X + a_{33}^{(2)}\right) + a_{31}^{*(1)} - \frac{\Omega_{c1}\Omega_{c2}}{d_{32}^*}a_{02}^{*(2)}\right], \tag{B4h}$$

$$a_{32}^{(2)} = \frac{1}{d_{32}}\left(\Omega_{c1}a_{03}^{*(2)} - \Omega_{c2}^*a_{02}^{(2)}\right), \tag{B4i}$$

where

$$A = -\frac{d_{32}^*M^*}{\Omega_{c1}^*}\left\{\frac{|\Omega_{c1}|^2\Omega_{c2}}{P}(N^* - N) - \frac{\Omega_{c1}\Omega_{c2}}{d_{32}^*N^*}\left[\frac{M^*|\Omega_{c1}|^2\Omega_{c2}}{P}(N^* - N) - \Omega_{c1}^*\right]\right\}, \tag{B5a}$$

$$B = \frac{d_{32}^* M^*}{\Omega_{c1}^*}\left\{\Omega_{c2}\frac{1}{i\Gamma_{10}}X + \frac{\Omega_{c2}Q}{i\Gamma_{10}P} + a_{31}^{*(1)} - \frac{\Omega_{c1}\Omega_{c2}}{d_{32}^* N^*}\left[M^*\Omega_{c2}\left(\frac{1}{i\Gamma_{10}X} + \frac{Q}{i\Gamma_{10}P}\right) + M^* a_{31}^{*(1)} - a_{21}^{(1)} - \Omega_{c1}^*\frac{1}{i\Gamma_{10}}X\right]\right\}, \quad \text{(B5b)}$$

$$M = \frac{\Omega_{c1}\Omega_{c2}}{d_{32}}\left(\frac{|\Omega_{c1}|^2}{d_{32}} + d_{03}^*\right)^{-1}, \quad \text{(B5c)}$$

$$N = d_{02} + \frac{\Omega_{c1}^*\Omega_{c2}^* M - |\Omega_{c1}|^2}{d_{32}}, \quad \text{(B5d)}$$

$$P = N^* M \Omega_{c1}^*\Omega_{c2}^* - N M^* \Omega_{c1}\Omega_{c2}, \quad \text{(B5e)}$$

$$Q = [-i|N|^2\Gamma_{20} - P + |\Omega_{c1}|^2(N^* - N)]X - i\Gamma_{10}\left[\Omega_{c1}^* N^*\left(M a_{31}^{(1)} - a_{21}^{*(1)}\right) - \text{c.c.}\right], \quad \text{(B5f)}$$

$$X = \frac{(\omega + d_{21})(\omega + d_{31})}{D} - \frac{(\omega + d_{21}^*)(\omega + d_{31}^*)}{D^*}. \quad \text{(B5g)}$$

With the solutions obtained above, we proceed to the third order of the expansion and obtain the envelope equation by a divergence-free condition

$$i\frac{\partial}{\partial z_2}F - \frac{1}{2}K_2\frac{\partial^2}{\partial t_1^2}F + W|F|^2 F e^{-2\overline{\alpha}z_2} = 0, \quad \text{(B6)}$$

where $\overline{\alpha} = \epsilon^{-2}\alpha$ [$\alpha \equiv \text{Im}(K)$] is the absorption coefficient, $K_2 = \partial^2 K/\partial\omega^2$ is the coefficient of group-velocity dispersion, and W is the coefficient of self-phase modulation, which reads

$$W = -\kappa_{01}\frac{S + \Omega_{c1}(\omega + d_{31})a_{02}^{*(2)} + \Omega_{c2}(\omega + d_{21})a_{03}^{*(2)}}{D}, \quad \text{(B7)}$$

where $S = (\omega + d_{21})(\omega + d_{31})(2a_{11}^{(2)} + a_{22}^{(2)} + a_{33}^{(2)})$. Combining the above two envelope Eqs. (B3) and (B6), we obtain Eq. (5) in the main text when returning to the original variables.

Because under the EIT condition the absorption of the probe pulse is largely suppressed, the imaginary parts of K_2 and W_2 are thus much smaller than their corresponding real parts. Neglecting these small imaginary parts in K_2 and W_2, we get the dimensionless nonlinear equation

$$i\frac{\partial U}{\partial s} - s_d\frac{\partial^2 U}{\partial\sigma^2} + 2|U|^2 U = i g_0 U, \quad \text{(B8)}$$

with $U = \epsilon F\exp(-i\alpha z)/U_0$, $s = z/(2L_\text{D})$, $\sigma = (t - z/V_g)/\tau_0$, $L_\text{D} = \tau_0^2/|\tilde{K}_2|$ (the tilde symbol denotes taking the real part), $s_d = \text{sgn}(\tilde{K}_2)$, and $g_0 = 2L_\text{D}/L_0$. Here $L_0 = 1/\text{Im}(K)$ is typical absorption length; L_D is typical dispersion length, which has been assumed to be equal to typical nonlinearity length $L_\text{NL} \equiv 1/(\tilde{W}U_0^2)$, and hence $U_0 = (1/\tau_0)\sqrt{|\tilde{K}_2|/\tilde{W}}$. Note that $\tilde{W}$ has been assumed to be positive, which is valid if both two-photon detunings Δ_2 and Δ_3 are negative, the case we consider here. For $U_0 = 2\pi \times 8.3$ MHz and the other system parameters the same as given in the main text, we have $L_\text{D} = 1.1$ cm, $L_0 = 46.3$ cm, and hence $g_0 = 0.05$. Since $s_d = -1$ and $ig_0 U$ is very small, one can get the approximated single bright soliton solution of Eq. (B8), i.e.,

$$U = \beta\,\text{sech}[\beta(\sigma - c_0 s - \sigma_0)] \times \exp\left[i\frac{c_0}{2}\sigma + i\left(\beta^2 - \frac{c_0^2}{4}\right)s - i\phi_0\right]. \quad \text{(B9)}$$

Here β, c_0, σ_0, and ϕ_0 are free parameters which determine the amplitude (temporal width), velocity, initial position, and initial phase of the soliton, respectively. When taking $\beta = 1$, $c_0 = 0$, $\sigma_0 = 0$, and $\phi_0 = 0$, the half Rabi frequency of the probe pulse corresponding to the solution (B9) is just that given by Eq. (6) after returning to the original variables.

Figure 5 shows the time evolution of the slow-light soliton by taking U as a function of t/τ_0 and $z/(2L_\text{D})$. The boundary condition at $z = 0$ is chosen to be $U = 0.8\,\text{sech}(0.8t/\tau_0)$ with $\tau_0 = 1.0 \times 10^{-7}$ s. We see that the soliton is very stable during propagation due to the balance between the dispersion and the Kerr nonlinearity in the system.

APPENDIX C: EXPRESSIONS OF PROBE PULSES FOR SOLITON MEMORY AND SPLITTING

For the problems of soliton memory and soliton splitting, it is not possible to get exact solutions of the MB Eqs. (2) and (3), because these equations not only are nonlinear ones (due to the coupling between light and atoms) but also have variable coefficients (due to the time-dependent control fields needed to implement the manipulation of the

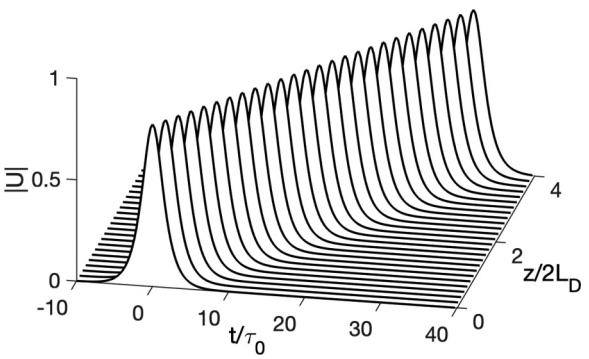

FIG. 5. Evolution of the slow-light soliton by taking U as function of t/τ_0 and $z/(2L_\text{D})$.

probe solitons). However, it is possible to provide approximated analytical solutions of the probe field in different time slots.

1. The case of soliton memory

In the case of the storage and retrieval (Sec. II.B.1 in the main text), the two control fields Ω_{c1} and Ω_{c2} are (or recover to) constant values in the time slots before the storage and after the retrieval of the slow-light soliton. In these time slots, the description by the envelope Eq. (5) in the main text is still valid. Thus one has the following solution for the probe pulse:

$$\Omega_p \approx \begin{cases} \frac{A_0}{\tau_0}\sqrt{\frac{|\tilde{K}_2|}{\tilde{W}}}\,\mathrm{sech}\big[\frac{1}{\tau_0}\big(t-\frac{z}{\tilde{V}_g}\big)\big]e^{i[\tilde{K}_0-1/(2L_\mathrm{D})]z}, \\ \quad \text{for } t < \mathrm{T_{off}}, \\ 0, \quad \text{for } \mathrm{T_{off}} < t < \mathrm{T_{on}}, \\ \frac{B_0}{\tau_0}\sqrt{\frac{|\tilde{K}_2|}{\tilde{W}}}\,\mathrm{sech}\big[\frac{1}{\tau_0}\big(t-\frac{z}{\tilde{V}_g}\big)\big]e^{i[\tilde{K}_0-1/(2L_\mathrm{D})]z+i\phi_0}, \\ \quad \text{for } t > \mathrm{T_{on}}, \end{cases}$$

where A_0 and B_0 are constants, ϕ_0 is a constant phase factor, $T_{\mathrm{off}} \equiv T^1_{\mathrm{off}} = T^2_{\mathrm{off}}$, and $T_{\mathrm{on}} \equiv T^1_{\mathrm{on}} = T^2_{\mathrm{on}}$.

2. The case of soliton splitting

The realization of the soliton beam splitter requires that initially the two control fields are switched on simultaneously, and then switched off and on in subsequent time slots [see Fig. 3(a) in the main text]. In the time slot $t < T^1_{\mathrm{off}_1}$, the two control fields are constants and the envelope of the probe pulse is described by Eq. (5), so it is a slow-light soliton given by Eq. (6). In the time slot $T^1_{\mathrm{on}_1} < t < T^1_{\mathrm{off}_2}$, the control field Ω_{c1} is switched on again but Ω_{c2} remains switched off, thus the four-level tripod system is reduced into a three-level Λ-type system (with Ω_p and Ω_{c1} coupling the levels $|0\rangle$, $|1\rangle$, and $|2\rangle$). In this case, due to the existence of the constant Ω_{c1}, the envelope of the probe pulse is still described by Eq. (5) but with $\Omega_{c2} = 0$. In the time slot $T^1_{\mathrm{off}_2} < t < T^2_{\mathrm{on}_1}$, the control field Ω_{c1} is switched off but Ω_{c2} is switched on again to a constant value; the four-level tripod system is thus converted into another three-level Λ-type system (with Ω_p and Ω_{c2} coupling the levels $|0\rangle$, $|1\rangle$, and $|3\rangle$). In this case, due to the constant Ω_{c2}, the envelope of the probe pulse is still described by Eq. (5) but with $\Omega_{c1} = 0$. That is to say, in the time slots of $t < T^1_{\mathrm{off}_1}$, $T^1_{\mathrm{on}_1} < t < T^1_{\mathrm{off}_2}$, and $t > T^2_{\mathrm{on}_1}$, the description by the envelope Eq. (5) in the main text is valid but with different control fields. Consequently, during the soliton splitting, the probe pulse can be written as the form

$$\Omega_p \approx \begin{cases} \frac{A_0}{\tau_0}\sqrt{\frac{|\tilde{K}_2|}{\tilde{W}}}\,\mathrm{sech}\big[\frac{1}{\tau_0}\big(t-\frac{z}{\tilde{V}_g}\big)\big]\,e^{i[\tilde{K}_0-1/2L_\mathrm{D}]z}, \\ \quad \text{for } t < T^1_{\mathrm{off}_1}, \\ 0, \text{ for } T^1_{\mathrm{off}_1} < t < T^1_{\mathrm{on}_1}, \\ \frac{B'_0}{\tau_0}\sqrt{\frac{|\tilde{K}'_2|}{\tilde{W}'}}\,\mathrm{sech}\big[\frac{1}{\tau_0}\big(t-\frac{z}{\tilde{V}'_g}\big)\big]\,e^{i[\tilde{K}'_0-1/2L'_\mathrm{D}]z+i\phi'_0}, \\ \quad \text{for } T^1_{\mathrm{on}_1} < t < T^1_{\mathrm{off}_2}, \\ 0, \text{ for } T^1_{\mathrm{off}_2} < t < T^2_{\mathrm{on}_1}, \\ \frac{B''_0}{\tau_0}\sqrt{\frac{|\tilde{K}''_2|}{\tilde{W}''}}\,\mathrm{sech}\big[\frac{1}{\tau_0}\big(t-\frac{z}{\tilde{V}''_g}\big)\big]\,e^{i[\tilde{K}''_0-1/2L''_\mathrm{D}]z+i\phi''_0}, \\ \quad \text{for } t > T^2_{\mathrm{on}_1}, \end{cases}$$

where A_0, B'_0, B''_0, ϕ'_0, and ϕ''_0 are constants. In the above expression,

$$K'(\omega) = \omega/c + \kappa_{10}(\omega + d_{21})/D', \tag{C1a}$$

$$K'_0 = K'(\omega)|_{\omega=0}, \tag{C1b}$$

$$V'_g = (\partial K'/\partial\omega)^{-1}, \tag{C1c}$$

$$K'_2 = \partial^2 K'/\partial\omega^2, \tag{C1d}$$

$$W' = \kappa_{01}\big[\Omega_{c1}a'^{(2)*}_{32} + (\omega + d_{21})\big(2a'^{(2)}_{11} + a'^{(2)}_{22}\big)\big]/D', \tag{C1e}$$

$$L'_\mathrm{D} = \tau'^2_0/|\tilde{K}'_2|, \tag{C1f}$$

$$D' = |\Omega_{c1}|^2 - (\omega + d_{21})(\omega + d_{01}), \tag{C1g}$$

and

$$K''(\omega) = \omega/c + \kappa_{10}(\omega + d_{31})/D'', \tag{C2a}$$

$$K''_0 = K''(\omega)|_{\omega=0}, \tag{C2b}$$

$$V''_g = (\partial K''/\partial\omega)^{-1}, \tag{C2c}$$

$$K''_2 = \partial^2 K''/\partial\omega^2, \tag{C2d}$$

$$W'' = \kappa_{01}\big[\Omega_{c2}a''^{(2)*}_{32} + (\omega + d_{31})\big(2a''^{(2)}_{11} + a''^{(2)}_{22}\big)\big]/D'', \tag{C2e}$$

$$L''_\mathrm{D} = \tau''^2_0/|\tilde{K}''_2|, \tag{C2f}$$

$$D'' = |\Omega_{c2}|^2 - (\omega + d_{31})(\omega + d_{01}). \tag{C2g}$$

Expressions of $a'^{(2)}_{jl}$ ($a''^{(2)}_{jl}$) can be obtained from that of $a^{(2)}_{jl}$ in Sec. IV described above by taking $\Omega_{c2} = 0$ ($\Omega_{c1} = 0$).

[1] R. Loudon, *The Quantum Theory of Light*, 3rd ed. (Oxford University, New York, 2000).

[2] M. O. Scully and M. S. Zubairy, *Quantum Optics* (Cambridge University, Cambridge, England, 2000).

[3] T. Wang, M. Koštrun, and S. Yelin, Multiple beam splitter for single photons, Phys. Rev. A **70**, 053822 (2004).

[4] B. S. Ham, Experimental demonstration of all-optical 1×2 quantum routing, Appl. Phys. Lett. **85**, 893 (2004).

[5] B. Wang, S. Li, H. Wu, H. Chang, H. Wang, and M. Xiao, Controlled release of stored optical pulses in an atomic ensemble into two separate photonic channels, Phys. Rev. A **72**, 043801 (2005).

[6] I. E. Mazets, Adiabatic pulse propagation in coherent atomic media with the tripod level configuration, Phys. Rev. A **71**, 023806 (2005).

[7] A. Joshi and M. Xiao, Generalized dark-state polaritons for photon memory in multilevel atomic media, Phys. Rev. A **71**, 041801(R) (2005).

[8] A. Raczyński, M. Rzepecka, J. Zaremba, and S. Zielińska-Kaniasty, Polariton picture of light propagation and storing in a tripod system, Opt. Commun. **206**, 73 (2006).

[9] A. Raczyński, J. Zaremba, and S. Zielińska-Kaniasty, Beam splitting and Hong-Ou-Mandel interference for stored light, Phys. Rev. A **75**, 013810 (2007).

[10] B. S. Ham, Observations of delayed all-optical routing in a slow-light regime, Phys. Rev. A **78**, 011808(R) (2008).

[11] Y. Xiao, M. Klein, M. Hohensee, L. Jiang, D. F. Phillips, M. D. Lukin, and R. L. Walsworth, Slow Light Beam Splitter, Phys. Rev. Lett. **101**, 043601 (2008).

[12] H.-H. Wang, A.-J. Li, D.-M. Du, Y.-F. Fan, L. Wang, Z.-H. Kang, Y. Jiang, J.-H. Wu, and J.-Y. Gao, All-optical routing by light storage in a Pr^{3+} : Y_2SiO_5 crystal, Appl. Phys. Lett. **93**, 221112 (2008).

[13] Y. Han, J. Xiao, Y. Liu, C. Zhang, H. Wang, M. Xiao, and K. Peng, Interacting dark states with enhanced nonlinearity in an ideal four-level tripod atomic system, Phys. Rev. A **77**, 023824 (2008).

[14] H.-H. Wang, Y.-F. Fan, R. Wang, D.-M. Du, X.-J. Zhang, Z.-H. Kang, Y. Jiang, J.-H. Wu, and J.-Y. Gao, Three-channel all-optical routing in a Pr^{3+} : Y_2SiO_5 crystal, Opt. Express **17**, 12197 (2009).

[15] X.-L. Song, A.-J. Li, L. Wang, Z.-H. Kang, J. Kou, B. Zhang, C.-L. Wang, Y. Jiang, and J.-Y. Gao, Storage and switching of multiple optical signals among three channels, Phys. Rev. A **79**, 053857 (2009).

[16] Y. Zhang, C. Zuo, H. Zheng, C. Li, Z. Nie, J. Song, H. Chang, and M. Xiao, Controlled spatial beam splitter using four-wave-mixing images, Phys. Rev. A **80**, 055804 (2009).

[17] J.-W. Gao, J.-H. Wu, N. Ba, C.-L. Cui, and X.-X. Tian, Efficient all-optical routing using dynamically induced transparency windows and photonic band gaps, Phys. Rev. A **81**, 013804 (2010).

[18] H. Wang, S. Li, Z. Xu, X. Zhao, L. Zhang, J. Li, Y. Wu, C. Xie, K. Peng, and M. Xiao, Quantum interference of stored dual-channel spin-wave excitations in a single tripod system, Phys. Rev. A **83**, 043815 (2011).

[19] Q.-Q. Bao, J.-W. Gao, C.-L. Cui, G. Wang, Y. Xue, and J.-H. Wu, Dynamic generation of robust and controlled beating signals in an asymmetric procedure of light storage and retrieval, Opt. Express **19**, 11832 (2011).

[20] D.-S. Ding, J.-H. Wu, Z.-Y. Zhou, B.-S. Shi, X.-B. Zou, and G.-C. Guo, Multiple image storage and frequency conversion in a cold atomic ensemble, Phys. Rev. A **87**, 053830 (2013).

[21] M. J. Lee, J. Ruseckas, C. Y. Lee, V. Kudriasov, K. F. Chang, H. W. Cho, G. Juzeliunas, and I. A. Yu, Experimental demonstration of spinor slow light, Nat. Commun. **5**, 5542 (2014).

[22] S.-J. Yang, X.-H. Bao, and J.-W. Pan, Modulation of single-photon-level wave packets with two-component electromagnetically induced transparency, Phys. Rev. A **91**, 053805 (2015).

[23] K. K. Park, T. M. Zhao, J. C. Lee, Y. T. Chough, and Y. H. Kim, Coherent and dynamic beam splitting based on light storage in cold atoms, Sci. Rep. **6**, 34279 (2016).

[24] S. Beck and I. E. Mazets, Propagation of coupled dark-state polaritons and storage of light in a tripod medium, Phys. Rev. A **95**, 013818 (2017).

[25] M. Fleischhauer, A. Imamoglu, and J. P. Marangos, Electromagnetically induced transparency: Optics in coherent media, Rev. Mod. Phys. **77**, 633 (2005).

[26] N. Sangouard, C. Simon, H. de Riedmatten, and N. Gisin, Quantum repeaters based on atomic ensembles and linear optics, Rev. Mod. Phys. **83**, 33 (2011).

[27] F. Bussiéres, N. Sangouard, M. Afzelius, H. de Riedmatten, C. Simon, and W. Tittel, Prospective applications of optical quantum memories, J. Mod. Opt. **60**, 1519 (2013).

[28] L. Barry and X. Yang, Waveguides, and Y junctions formed in bulk media by using dark spatial solitons, Opt. Lett. **17**, 496 (1992).

[29] Z. Chen, M. Mitchell, and M. Segev, Steady-state photorefractive soliton-induced Y-junction waveguides and high-order dark spatial solitons, Opt. Lett. **21**, 716 (1996).

[30] A. Guo, M. Henry, G. J. Salamo, M. Segev, and G. L. Wood, Fixing multiple waveguides induced by photorefractive solitons: Directional couplers and beam splitters, Opt. Lett. **26**, 1274 (2001).

[31] K. Steiglitz, Soliton-guided phase shifter and beam splitter, Phys. Rev. A **81**, 033835 (2010).

[32] K. Steiglitz, Making beam splitters with dark soliton collisions, Phys. Rev. A **82**, 043831 (2010).

[33] A. Madani, J. Beeckmanc, and K. Neytsc, An experimental observation of a spatial optical soliton beam and self splitting of beam into two soliton beams in chiral nematic liquid crystal, Opt. Commun. **298–299**, 222 (2013).

[34] S. Pu, C. Hou, K. Zhan, and Y. Du, Beam splitters in inhomogeneous nonlocal media, Phys. Scr. **86**, 025404 (2012).

[35] H. Sakaguchi and B. A. Malomed, Matter-wave soliton interferometer based on a nonlinear splitter, New J. Phys. **18**, 025020 (2016).

[36] R. W. Boyd, *Nonlinear Optics*, 3rd ed. (Academic, New York, 2008).

[37] D. A. Steck, Rubidium 87 D Line Data, https://steck.us/alkalidata/.

[38] ω is a deviation (sideband) frequency of the probe pulse, generated by the interaction with the atomic gas. Thus the frequency and wave number of the probe pulse in the atomic medium are given by $\omega_p + \omega$ and $k_p + K_p(\omega)$, respectively.

[39] Y. Wu and L. Deng, Ultraslow Optical Solitons in a Cold Four-State Medium, Phys. Rev. Lett. **93**, 143904 (2004).

[40] G. Huang, L. Deng, and M. G. Payne, Dynamics of ultraslow optical solitons in a cold three-state atomic system, Phys. Rev. E **72**, 016617 (2005).

[41] Y. Wu and L. Deng, Ultraslow bright and dark optical solitons in a cold three-state medium, Opt. Lett. **29**, 2064 (2004).

[42] A. I. Lvovsky, B. C. Sanders, and W. Tittel, Optical quantum memory, Nat. Photon. **3**, 706 (2009).

[43] I. Novikova, R. L. Walsworth, and Y. Xiao, Electromagnetically induced transparency-based slow and stored light in warm atoms, Laser Photon. Rev. **6**, 333 (2012).

[44] Y. Chen, Z. Bai, and G. Huang, Ultraslow optical solitons and their storage and retrieval in an ultracold ladder-type atomic system, Phys. Rev. A **89**, 023835 (2014).

[45] Y. Chen, Z. Chen, and G. Huang, Storage and retrieval of vector optical solitons via double electromagnetically induced transparency, Phys. Rev. A **91**, 023820 (2015).

[46] D. Xu, Z. Chen, and G. Huang, Ultraslow weak-light solitons and their storage and retrieval in a kagome-structured hollow-core photonic crystal fiber, Opt. Express **25**, 19094 (2017).

[47] A. Jeffery and T. Kawahawa, *Asymptotic Method in Nonlinear Wave Theory* (Pitman, London, 1982).

[48] K. F. Reim, J. Nunn, X.-M. Jin, P. S. Michelberger, T. F. M. Champion, D. G. England, K. C. Lee, W. S. Kolthammer, N. K. Langford, and I. A. Walmsley, Multipulse Addressing of a Raman Quantum Memory: Configurable Beam Splitting and Efficient Readout, Phys. Rev. Lett **108**, 263602 (2012).